Earth and Planetary Science Letters 272 (2008) 610–619

Contents lists available at ScienceDirect

Earth and Planetary Science Letters

journal homepage: www.elsevier.com/locate/epsl

# Modeling the distribution of Nd isotopes in the oceans using an ocean general circulation model

Kevin M. Jones [a,b,*], Samar P. Khatiwala [a], Steven L. Goldstein [a,b], Sidney R. Hemming [a,b], Tina van de Flierdt [b,c,1]

[a] Lamont-Doherty Earth Observatory, 61 Route 9W, Palisades, NY 10964, USA
[b] Department of Earth and Environmental Sciences, Columbia University, 16 Rt. 9W, Palisades, NY 10964, USA
[c] Department of Earth Science and Engineering, Imperial College London, South Kensington Campus, London SW7 2AZ, UK

ARTICLE INFO

*Article history:*
Received 19 November 2007
Received in revised form 20 May 2008
Accepted 21 May 2008
Available online 5 June 2008

Editor: H. Elderfield

*Keywords:*
Neodymium isotopes
seawater
ocean modeling
ocean circulation
general circulation model

ABSTRACT

Nd isotopic compositions of authigenic phases in marine archives are increasingly used as a tracer of past changes in ocean circulation. Such applications assume that water masses are "tagged" with distinct Nd isotope compositions in source regions and that away from these regions the Nd isotope ratios observed in deep waters mainly reflect water mass mixing. However, the degree to which the simple assumption of "quasi-conservative mixing" reflects the complicated reality of general circulation in the oceans is not well understood.

Here, we present numerical simulations of the Nd isotope distribution in seawater using an offline ocean general circulation model (OGCM), treating the Nd isotopic composition of seawater as a conservative tracer. Nd isotope data from modern surface waters are used to generate an interpolated map of Nd isotope compositions for the entire surface ocean. This map is treated as a fixed surface boundary condition that is propagated into the interior ocean by the advective–diffusive transport of the ocean model until a steady state is reached. This treatment of Nd isotopes was chosen because it mimics the behavior of well-known and well-understood conservative tracers, such as potential temperature and salinity. The model results for all non-surface grid points are then compared to published data.

This simple approach produces Nd isotope estimates for North Atlantic Deep Water that are consistent with observations, but produces values lower than observed in the deep Pacific and Southern Oceans, indicating the need for a source of radiogenic Nd directly to the deep Pacific Ocean. Sensitivity tests show this to be a robust result. By fixing the return flow of the Pacific Ocean to the Southern Ocean with Nd isotope ratios that are consistent with modern observations, the model results are brought into close agreement with a majority of the available data. With the addition of a deep Pacific source of radiogenic Nd, more than half of the simulated values from the interior ocean fall within one $\varepsilon$-unit of the corresponding observations. Our results thus indicate that the deep Pacific Ocean requires a source of radiogenic Nd in addition to inputs to the surface ocean, and that when the deep waters of the North Atlantic and North Pacific are set with realistic values, a majority of intermediate areas are consistent with quasi-conservative mixing of these two end-members.



## 1. Introduction

The authigenic (seawater-derived) neodymium (Nd) isotopic composition of marine archives is increasingly used to study changes in ocean circulation in the context of climate change on millennial and longer time-scales. Its usefulness as a tracer of ocean circulation is a consequence of its variable isotopic composition in the oceans, which reflects sources of different crustal age, and its estimated residence time (200–2000 years: Goldstein and O'Nions, 1981; Piepgras and Wasserburg, 1983; Jeandel, 1993; Tachikawa et al., 1999; Tachikawa et al., 2003) being close to, or shorter than the mixing time of the oceans (~1500 years e.g. Broecker and Peng, 1982).

The earliest Nd isotope studies of seawater and authigenic Fe–Mn crusts and nodules showed that the lowest Nd isotope ratios are in the North Atlantic, reflecting the old continental crust surrounding the basin, while the highest values are in the north Pacific, reflecting input from young volcanism along its rim; and intermediate values occur in the Indian Ocean (Piepgras et al., 1979; Piepgras and Wasserburg, 1980; Goldstein and O'Nions, 1981). Subsequent studies showed that deep waters in all ocean basins show variations consistent with water mass mixing (summarized in: Frank, 2002; Goldstein and Hemming, 2003). In particular, Nd isotope ratios in the deep Atlantic show variations consistent with mixing of North Atlantic Deep Water (NADW) and Circum-Antarctic water masses, and values in the Circum-Antarctic are broadly consistent with mixing of North Atlantic

* Corresponding author.
*E-mail address:* kjones@ldeo.columbia.edu (K.M. Jones).
[1] Tina van de Flierdt has changed location from LDEO to Imperial College in the UK.

0012-821X/$ – see front matter © 2008 Elsevier B.V. All rights reserved.
doi:10.1016/j.epsl.2008.05.027

and North Pacific water masses. These observations have been taken to imply a relatively simple system where seawater Nd isotopes are imprinted mainly in the North Atlantic and North Pacific, and where the Nd isotopes in deep waters can be regarded as a quasi-conservative tracer (i.e. a tracer that approximates conservative behavior) of water masses and thus a potential tool for studying changes in ocean circulation through time (Piepgras and Wasserburg, 1982; Rutberg et al., 2000; Frank, 2002; Goldstein and Hemming, 2003; Martin and Scher, 2004; Piotrowski et al., 2004; Vance et al., 2004; Piotrowski et al., 2005; van de Flierdt et al., 2006). However, the extent to which this simple scenario of quasi-conservative mixing applies to the ocean remains unclear. Potential complicating factors include input from rivers and dust, exchange at continental margin boundaries, and fluxes from the ocean-sediment interface (e.g. Frank, 2002; Goldstein and Hemming, 2003; Lacan and Jeandel, 2005a; Johannesson and Burdige, 2007).

A major obstacle to a more complete understanding of the marine Nd cycle is the lack of a truly global dataset for the modern oceans, as many of the modern data are from only a few regions of the ocean. Nevertheless, even within the constraints of sparse data, a better understanding of the sources, and internal cycling of Nd may be reached through ocean modeling.

In this study, we use an ocean general circulation model (OGCM) to simulate the distribution of Nd isotopes in seawater, and use the misfit between the model and the measured data to guide our understanding of the present day Nd isotope distribution in the ocean. In this initial attempt, we take the simple approach of treating the Nd isotopic composition of seawater as a conservative tracer and assuming constant concentrations of Nd in the oceans, as did Arsouze et al. (2007). In the first model run, Nd isotope data from the modern surface ocean were used as a fixed surface boundary condition, then transported and mixed according to the flow characteristics of the OGCM until the interior ocean reached a steady state. Results showed substantial disagreement between the model output and data, particularly in the Pacific and Southern Oceans where modeled Nd isotopes were too low. In the second run we introduce a more radiogenic source of Nd in the Pacific, which brings the model into good agreement with the data. These results suggest that the observed Nd isotope ratios of the waters in the deep North Pacific Ocean are influenced by an internal source of radiogenic Nd. Also, when the deep water end-member in the North Pacific is fixed with realistic $\varepsilon_{Nd}$ values, the distribution of Nd isotopes in the global deep oceans is consistent with quasi-conservative mixtures of Nd from the North Atlantic and the deep Pacific Ocean.

## 2. Background

$^{143}$Nd is produced by α-decay of $^{147}$Sm ($\lambda = 6.54\times10^{-12}$ a$^{-1}$, $t_{1/2} = 1.06\times10^{11}$ a). Nd isotope ratios are often reported as $^{143}$Nd/$^{144}$Nd or $\varepsilon_{Nd}$ (the deviation from a chondritic uniform reservoir, CHUR, representing the "bulk Earth", in parts per ten thousand). That is, $\varepsilon_{Nd} = [(R_s/R_{CHUR} - 1)\times10^4]$, where $R_s$ and $R_{CHUR}$ are the $^{143}$Nd/$^{144}$Nd ratios of the measured sample and CHUR, respectively. The present-day value of CHUR is 0.512638 (Jacobsen and Wasserburg, 1980). The continental crust has a lower Sm/Nd than the mantle, and thus the mantle (and young mantle-derived magmas) generally have $^{143}$Nd/$^{144}$Nd ratios higher than the bulk Earth, or positive $\varepsilon_{Nd}$, while old crustal rocks have $^{143}$Nd/$^{144}$Nd ratios lower than the bulk Earth, or negative $\varepsilon_{Nd}$, and become more progressively negative with increasing age.

In the present day ocean general circulation system, warm, salty waters from the subtropical gyre in the North Atlantic cool as they move northward along the western boundary, losing buoyancy and making these waters dense enough to initiate deep convection. Through a process of mixing multiple source waters from the ocean surface, along with some exchange of Nd between water and sediments near Greenland (Lacan and Jeandel, 2005b) NADW is imparted with a characteristic $\varepsilon_{Nd}$ value of −13.5±0.5 (Piepgras and Wasserburg, 1987). As NADW is exported southward, it is sandwiched by northward flowing Antarctic Intermediate Water (AAIW) and Antarctic Bottom Water (AABW) from the Southern Ocean, with $\varepsilon_{Nd}$ characteristically between −7 and −9 (Piepgras and Wasserburg, 1982; Jeandel, 1993). Intermediate mixtures of these water masses in depth profiles show intermediate $\varepsilon_{Nd}$ values consistent with quasi-conservative mixing (Goldstein and Hemming, 2003).

The inflow of AABW into the Pacific Ocean can be seen through the pattern of $\Delta^{14}$C values of the deep Pacific (Schlosser et al., 2001), and this pattern is mimicked by the spatial distribution of $\varepsilon_{Nd}$ values in ferromanganese crusts and nodules from the same region (Albarède and Goldstein, 1992). There are only two published analyses of seawater $\varepsilon_{Nd}$ in the deep South Pacific Ocean (20°S, 160°W, 4500 m and 48°S, 83°W, 3900 m: Piepgras and Wasserburg, 1982), but the $\varepsilon_{Nd}$ values of −8.1 and −7.9, respectively, are consistent with derivation from the Southern Ocean. All remaining Nd isotope analyses of the deep Pacific Ocean are from sites located north of the equator, where the water column is dominated by Pacific Deep Water (PDW, also called Pacific Common Water), with $\varepsilon_{Nd}$ values typically ranging between −3 and −6 (Piepgras and Wasserburg, 1980; Piepgras and Jacobsen, 1988; Shimizu et al., 1994; Amakawa et al., 2004; Vance et al., 2004). This water mass is thought to be derived from a mixture of deep, bottom and intermediate water masses formed in other oceans and intermediate waters formed in the Pacific (Bearman, 2002). Some studies have analyzed the importance of potential sources of Nd to the Pacific Ocean, including eolian dust and circum-Pacific arc volcanism (e.g. Nakai et al., 1993; Jones et al., 1994; Amakawa et al., 2004; van de Flierdt et al., 2004). While the process whereby Nd is added to the Pacific is debated, there is general consensus that the high $\varepsilon_{Nd}$ values of deep North Pacific waters reflect input from Circum-Pacific volcanism.

Previous efforts to use numerical models to better understand the cycle of Nd in the ocean focused on using Nd isotope and concentration data to balance the budget of Nd in the ocean. Bertram and Elderfield (1993) used a multi-box model to demonstrate an apparent need for large particle-water exchange fluxes to balance the budget of Nd in the ocean. Tachikawa et al. (2003) used a 10-box model to estimate exchange fluxes of Nd throughout the ocean, and concluded that the flux of Nd from rivers and aerosols is too low by almost an order of magnitude to account for the distribution of Nd isotope values in the ocean. They inferred that a 'missing source' of Nd must exist, possibly along the continental margins.

A drawback of box models is a lack of spatial resolution, since each box describes an enormous region with a single representative tracer value, even while the data within a box may be heterogeneous. In contrast, OGCMs have the advantage of higher spatial resolution and a dynamically consistent circulation and can, in principle, better represent the observed heterogeneity and more localized sources and sinks. The recent work of Arsouze et al. (2007) also used an OGCM to model Nd isotopes in the oceans, treating the Nd isotope composition of seawater as a conservative tracer and assuming constant concentrations. They focused on the question of whether a ubiquitous continental margin source of Nd can explain the global distribution of Nd isotopes in the modern oceans. The model allows for Nd isotope exchange between seawater and the rock surrounding the ocean basin over short timescales ("boundary exchange"). They concluded that an exchange timescale that decreased exponentially with depth best reproduces the observed $\varepsilon_{Nd}$ distribution. While their results were able to reproduce the Nd isotopic composition of NADW, they found significant offsets from measured Nd isotope data in the deep parts of ocean basins other than the North Atlantic.

## 3. Methods

### 3.1. Model description

To simulate the distribution of $\varepsilon_{Nd}$, we use an "offline" ocean circulation model based on the "transport matrix method" (TMM), a recently developed computational framework for efficiently simulating passive tracers in the ocean (Khatiwala et al., 2005; Khatiwala, 2007). The essential idea is that the discrete tracer transport operator of a GCM can be written as a sparse matrix, which may be efficiently constructed by "probing" the GCM (with idealized basis functions). This empirical approach ensures that the circulation embedded in the transport matrix (TM) accurately represents the complex 3-dimensional advective–diffusive transport (including all sub-grid scale parameterizations) of the underlying GCM. Once the matrix has been derived, the GCM can be dispensed with and simulating a tracer is reduced to a sequence of simple matrix-vector products. One of the key advantages of using the TMM is that it allows us to directly compute steady state solutions of the tracer equations without the need for lengthy transient integrations, as would be required with an OGCM or a conventional offline tracer model. Specifically, given surface boundary conditions and (optionally) interior source/sink terms, the steady state tracer distribution satisfies a linear system of equations that can be readily solved using software such as MATLAB. In the case where there is a fixed boundary, at the surface or otherwise, and no sources or sinks, the steady-state solution for all interior points is: $c_I=(I-A_i^I A_e^I)^{-1}(A_i^I B_e+B_i)c_B$; where $c_I$ and $c_B$ are vectors containing the interior and boundary concentrations, $A_i^I$ and $A_e^I$ are the implicit and explicit interior transport matrices, and $B_i$ and $B_e$ are the implicit and explicit boundary transport matrices, respectively (Khatiwala, 2007).

The TM used in this study was derived from a seasonally forced, global configuration of the MIT ocean model, a state-of-the-art primitive equation model (Marshall et al., 1997). The MIT GCM features a variety of parameterizations to represent unresolved processes, including isopycnal thickness diffusion (Gent and McWilliams, 1990) to represent the effect of mesoscale eddies. The configuration used here has a horizontal resolution of 2.8° and 15 vertical levels, and is forced with monthly mean climatological fluxes of momentum (Trenberth et al., 1989) and heat (Jiang et al., 1999). In addition, surface temperature and salinity are weakly restored to the 1998 (Levitus) World Ocean Atlas Climatology (Conkright et al., 1998a,b). To compute steady state solutions of the tracer equations with the TMM, the GCM was first integrated for 5000 years to equilibrium, following which an annual mean transport matrix was derived.

This version of the model has previously been used as MIT's contribution to the Ocean Carbon Model Inter-comparison Project Phase 2 (OCMIP-2), and further details, including an extensive discussion of its ability to reproduce observed CFC and radiocarbon distributions, can be found in Dutay et al. (2002)and Matsumoto et al. (2004). Briefly, the model tends to be more rapidly ventilated in both the North Pacific and subpolar North Atlantic, compared with observations, while it has relatively weak bottom water ventilation around Antarctica. These deficiencies in the model circulation are not atypical of coarse resolution GCMs.

To evaluate the sensitivity of our results to the circulation, we also perform a limited number of sensitivity experiments using an annual mean TM derived from a 1° resolution global configuration of the MIT GCM with 23 vertical levels. The model is forced with a monthly mean climatology of heat, freshwater, and momentum fluxes derived from the ECCO-GODAE ("Estimating the Circulation and Climate of the Ocean-Global Ocean Data Assimilation Experiment") data-assimilation project (Wunsch and Heimbach, 2007). As discussed by Wunsch and Heimbach (2007), the ECCO-GODAE approach involves adjusting air-sea fluxes to bring the model into consistency with a wide variety of hydrographic, velocity, and sea-surface height observations for the period 1992–2004. The circulation of this model is thus believed to represent a more robust estimate of the ocean circulation than the coarser 2.8° model. However, since the resulting TM is over 10 times larger, we only perform a limited number of experiments with it.

### 3.2. Construction of surface boundary condition

The main input to the model is the spatial distribution of $\varepsilon_{Nd}$ at the ocean surface. The principal challenge in constructing this boundary condition is the paucity of data in large parts of the world ocean. For example, there are only some 600 published water column measurements of $\varepsilon_{Nd}$, and these are focused in the North Atlantic and western North Pacific. Furthermore, only a small fraction of these data were measured in the surface ocean. The data used here are published seawater analyses of Nd isotopes based on the compilation of Goldstein and Hemming (2003) with additional compilation by Francois Lacan and Tina van de Flierdt (http://www.legos.obs-mip.fr/fr/equipes/geomar/results/database_may06.xls). The full list of references is given in the supplementary material. Consequently, to interpolate the sparse data onto the model grid, we were forced to adopt a somewhat *ad hoc* procedure that is a combination of simple spline interpolation, prescribing values for much of the Southern Ocean where few data exist, and using the TM to fill in gaps in a manner consistent with ocean circulation.

Specifically, we start by assigning the Nd isotope data to the nearest ocean model grid cell. Data located at depths greater than the lower boundary of the deepest model layer were assigned to the deepest layer (centered at 4855 m). When more than one observation fell within a single grid box, the average was taken and assigned to that box. Of the ~53,000 model grid boxes, observations were available for only 402 boxes. Of these, only 82 are from the surface layer (0–50 m), and the remaining observations are located in the interior ocean (>50 m). For the next step we applied a bi-harmonic spline (Sandwell, 1987) to interpolate the entire ocean surface using only the data from the upper 50 m of the ocean. Since this produced extreme local maxima and minima in the surface ocean outside the range of observed data in areas distant from locations with measured data, we only retained interpolated values that were within one grid cell of a measured data-point. This scheme of interpolation and retention of certain points was done to increase the number of gridpoints with defined Nd isotope ratios in the surface ocean.

A very important but difficult area to interpolate is the Southern Ocean because there exists only a single published surface water (≤50 m) value ($\varepsilon_{Nd}$=−9.1: Piepgras and Wasserburg, 1982) and one measurement from the Ross Sea mentioned in an abstract ($\varepsilon_{Nd}$=−8.9: Tazoe et al., 2006). For this region, we assigned a value of −8.9 to all grid points south of 60°S. This value is consistent with the two available observations, and is also close to the value of −8.5 assumed for the southern ocean by Tachikawa et al. (2003). Finally, we applied the advective–diffusive flow embedded within the TM to fill in the remaining surface grid points. The TM was used so that all remaining gridpoints were filled in with values consistent with the flow characteristics of the surface ocean. This yields an interpolated surface (Fig. 1) containing patterns consistent with ocean circulation, including zonal banding in the Southern Ocean, visible western boundary currents and a gradient between the Indian and Pacific Oceans at the Indonesian Throughflow.

### 3.3. Model uncertainties

As noted previously, an unavoidable source of uncertainty when trying to model Nd isotopes in the modern ocean is the lack of a global dataset. The scarcity of data greatly complicated the interpolation and extrapolation of surface Nd isotope values to empty model surface grid cells. We explored the possibility of using a coarser model, but

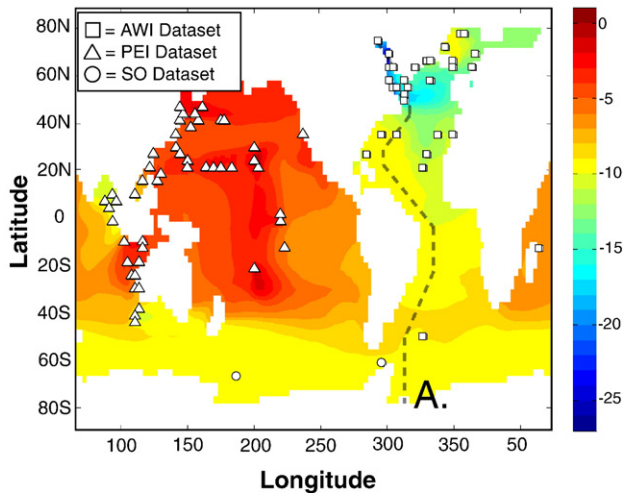


**Fig. 1.** Interpolated $\varepsilon_{Nd}$ of the surface ocean on the model grid. This map serves as the model fixed surface boundary, which is propagated into the interior ocean by the flow characteristics of the model. This map is constructed namely on the basis literature data, which are shown as squares, triangles, and circles depending on their geographic location: Atlantic–West Indian Ocean (AWI) are squares; Pacific–East Indian Ocean (PEI) are triangles; and Southern Ocean (SO) are circles. The location of the Western Atlantic Basin profiles in Fig. 4 is shown by the dashed line labeled 'A'.

even a significant reduction in the grid resolution failed to alleviate this problem because observations are not uniformly spaced.

Apart from the data paucity, additional uncertainty results from the fact that the model effectively assumes constant concentration of Nd throughout the oceans. As a result, a mixture of water masses with different Nd concentrations will lead to offsets between modeled and measured $\varepsilon_{Nd}$. However, we estimate that the effects of variable concentrations on the outcome of our modeling experiment are small because for waters deeper than 900 m, ≈90% of the Nd concentrations fall within a factor of two of each other (Goldstein and Hemming, 2003; Lacan and Jeandel, 2005a). Given the deep water masses at the edges of the observed Nd isotope spectrum (NADW and PDW; $\varepsilon_{Nd} \approx -13.5$ and −4, respectively), a 50–50 mixture and a factor of two concentration difference creates a maximum offset of ~1.6 $\varepsilon$-units. Thus, the error propagated into the model results by assuming uniform Nd concentrations should typically be less than ~1.6 $\varepsilon$-units.

We also considered the possibility of directly incorporating concentration data into our modeling approach by interpolating the available concentration data onto the model grid and modeling $^{143}$Nd and $^{144}$Nd separately. This approach would eliminate the uncertainty associated with assuming the same concentrations throughout. However, only about a third of the seawater samples with isotope measurements have accompanying concentration measurements, and this lack of paired concentration/isotope composition data further exacerbates the problem of poor data coverage. So, we decided to accept the uncertainties associated with the assumption of constant concentrations in order to maximize our data coverage.

We also must consider biases related to errors in the circulation of the OGCM. As mentioned above, the model used here has a general tendency to over ventilate. Specifically, while ventilation of NADW is reasonably realistic (Matsumoto et al., 2004), both CDW and PDW are more ventilated than observations would suggest (The problem is worse for CDW than PDW). Over ventilation of CDW over PDW could indicate that not enough waters from the surface Pacific are being incorporated into the deep waters of the North Pacific in this model. The potential of errors in the model circulation must be considered.

### 3.4. Experiment descriptions and data grouping

We carried out two sets of experiments. In the first experiment (Exp-1), we use the TMM with a prescribed surface distribution of $\varepsilon_{Nd}$ to compute the steady-state distribution for the interior ocean that would result if Nd inputs existed only in the surface ocean. The results from the first experiment (see Sections 4.1 and 4.2) demonstrated a need to introduce an additional source of Nd in the Pacific Ocean at depth. So, in a second experiment (Exp-2), we introduce a radiogenic water mass with Nd isotope ratios similar to those observed in the deep Pacific Ocean. This is accomplished by identifying grid points in this part of the ocean and fixing them all to a single value, which amounts to the introduction of another fixed boundary, in addition to the surface. We then use the TMM to compute the steady-state interior solution.

To compare model simulations with observations, we grouped the data into three sets: (1) Pacific-East Indian Ocean (PEI; $n=128$); (2) Atlantic-West Indian Ocean (AWI; $n=176$); and (3) Southern Ocean (SO; $n=16$). Indian Ocean data were appended to the AWI and PEI data sets because the Nd isotope variations in the Western Indian Ocean are similar to those of the Atlantic, while the Eastern Pacific Ocean Nd isotope variations resemble that of the Pacific. The three individual data groups were also divided by depth into subgroups that correspond to shallow, intermediate, deep, and bottom waters (50–550, 550–1820, 1820–3890 and 3890–5280 m, respectively). The division of the data into these depth ranges was chosen to coincide with boundaries between depth layers of the model grid.

## 4. Results and sensitivity tests

### 4.1. Experiment 1: fixed surface boundary condition with no internal sources

For Exp-1, with a prescribed surface distribution of Nd isotope values and no other sources of Nd, more than 70% of the model results for the interior ocean are within 3.0 $\varepsilon$-units of seawater Nd isotope data. However, the extent to which the model accurately simulates the measured data varies significantly by ocean basin (Figs. 2, 3a, and b). For example, the difference between data and model output [$\Delta\varepsilon_{Nd} = \varepsilon_{Nd}$(observed) − $\varepsilon_{Nd}$(modeled)] for the AWI and PEI datasets are quite different from each other (Figs. 3a, b). For AWI, $\Delta\varepsilon_{Nd}$ values are normally distributed about a mean close to zero with a standard deviation less than two $\varepsilon$-units (mean = 0.7 ± 1.8 $\varepsilon$-units; Table 1). The

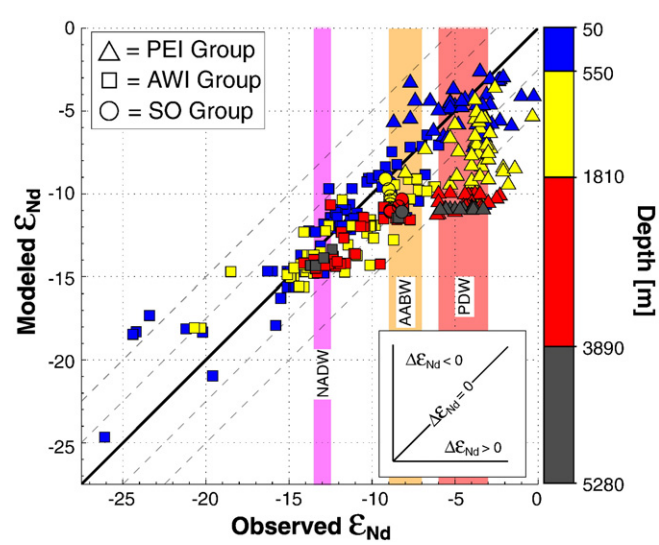


**Fig. 2.** Observed $\varepsilon_{Nd}$ versus modeled $\varepsilon_{Nd}$ for model grid points from depths greater than 50 m color-coded according to depth. The diagonal lines represent lines of equal $\Delta\varepsilon_{Nd}$ in 2.5 $\varepsilon$-unit intervals. The purple, orange, and red bars represent the typical ranges of $\varepsilon_{Nd}$ values for NADW, AABW, and PDW, respectively. The $\Delta\varepsilon_{Nd}$ values for the deep and bottom PEI group with measured $\varepsilon_{Nd}$ values similar to PDW are all skewed toward positive values. The $\Delta\varepsilon_{Nd}$ values for the deep and bottom SO group and AWI samples with measured $\varepsilon_{Nd}$ values similar to that exported from the Southern Ocean are also skewed toward positive $\Delta\varepsilon_{Nd}$ values.

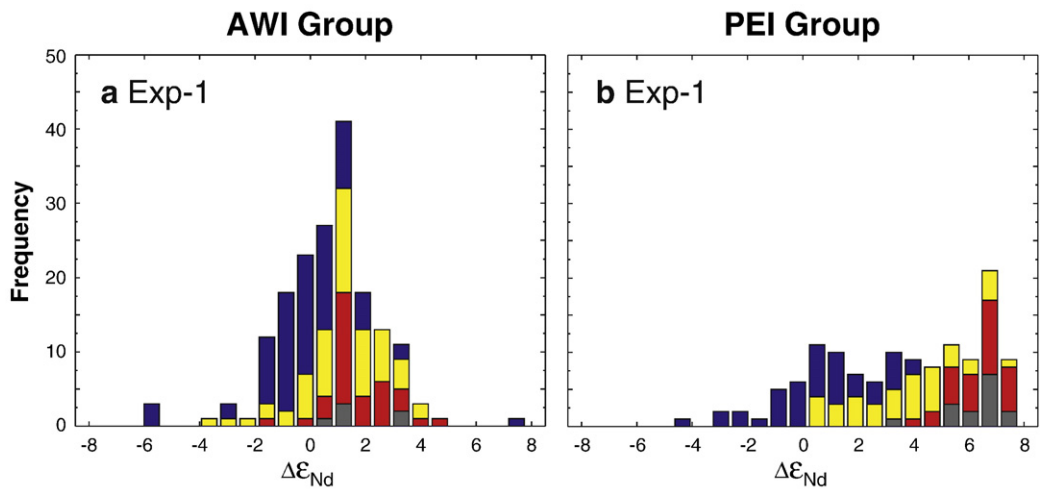


**Fig. 3.** Grouped histograms of model results showing the distributions of $\Delta\varepsilon_{Nd}$ values [$\Delta\varepsilon_{Nd}=\varepsilon_{Nd}$(observed)$-\varepsilon_{Nd}$(modeled)] for AWI (panel a) and PEI datasets (panel b) for Exp-1. The histograms are colored according to the depths listed in the text and shown in the color bar of Fig. 2 (shallow = blue; intermediate = yellow; deep = red; bottom = gray).

conformity between model results and measured seawater data for the AWI group breaks down to some degree at depth, where both deep and bottom depth ranges have means that are slightly more than one standard deviation higher than zero ($\text{mean}_{deep}=1.8\pm1.2$ $\varepsilon$-units, $\text{mean}_{bottom}=1.6\pm1.1$ $\varepsilon$-units).

The Exp-1 results for the PEI group do not show a normal distribution, but instead all layers other than the shallow depth range have mean $\Delta\varepsilon_{Nd}$ values significantly and progressively higher than zero (Table 1, Fig. 3b). The deep and bottom depth ranges of the PEI data group display the maximum averaged offsets seen in any data group. Investigation into specific regions within the PEI dataset shows that this offset is also observed in the Eastern Indian Ocean Data, showing that the offset can be observed on both sides of the Indonesian Arc.

The Exp-1 model output for the SO group as a whole also displays a mean positive $\Delta\varepsilon_{Nd}$ value (mean = 1.5 ± 0.8 $\varepsilon$-units). Furthermore, the mean $\Delta\varepsilon_{Nd}$ value increases with depth from 0.7 $\varepsilon$-units in the shallow to 2.9 $\varepsilon$-units for the bottom depth range. Investigation into individual data points from selected profiles in the Western Atlantic Basin shows that the deepest observations from the South Atlantic Ocean have observed $\varepsilon_{Nd}$ values consistent with AABW, and show offsets between the modeled and observed data that are similar to those of the deep Southern Ocean (Fig. 4).

### 4.2. Sensitivity of Experiment-1 to surface interpolation

Conservative transport of the interpolated surface $\varepsilon_{Nd}$ values in Exp-1 does not simulate the observed $\varepsilon_{Nd}$ values of the deep Pacific. This may be because our surface interpolation relies on a very sparse dataset, making it possible that the Exp-1 results could be heavily dependent upon areas where our interpolation is deficient. One such area of concern is the North Pacific, which may play a significant role in creating the observed $\varepsilon_{Nd}$ values for the deep Pacific.

We tested the sensitivity of model simulated $\varepsilon_{Nd}$ values for the North Pacific by altering the surface $\varepsilon_{Nd}$ values for all gridpoints in the North Pacific (north of 20°N) to values ranging between −6 to +24, running the simulation, and calculating the $\Delta\varepsilon_{Nd}$ values where data exist. We divided the data into a set of depth ranges similar to the those previously described in Section 3.4 with an additional subdivision added in the surface and intermediate waters to better monitor the sensitivity of model gridpoints at depths associated with NPIW to the surface ocean. The data were divided into surface (50–220 m: $n=12$), North Pacific Intermediate Water (220–790 m: $n=25$), intermediate waters (790–1810 m: $n=23$), deep waters (1810–3890 m: $n=23$) and bottom waters (>3890 m: $n=14$). A useful measure of sensitivity of these depth ranges to the interpolated $\varepsilon_{Nd}$ values for the North Pacific is to calculate the slope of line on a plot of $\Delta\varepsilon_{Nd}$ values versus interpolated $\varepsilon_{Nd}$ values for the surface North Pacific.

The results of this test show the sensitivities of different depth layers of the OGCM to the interpolated $\varepsilon_{Nd}$ values for the surface North Pacific (Fig. 5). The surface (50–220 m) and North Pacific Intermediate Water (220–790 m) depth ranges are most sensitive to the surface interpolation, with slopes of −1.00 and −0.83, respectively. The deeper intermediate waters (750–1810 m) are also sensitive to the interpolation (slope ~−0.28), but require an interpolated value for the North

**Table 1**
Model results for Exp-1 (no internal sources) and Exp-2 (deep Pacific internal source) showing the mean $\Delta\varepsilon_{Nd}$ [$\Delta\varepsilon_{Nd}=\varepsilon_{Nd}$(observed)$-\varepsilon_{Nd}$(modeled)] values ($x$) and standard deviation ($s$) for the bulk and depth differentiated data groups

| Experiment | Depth group | Depth range (m) | PEI | | AWI | | SO | |
|---|---|---|---|---|---|---|---|---|
| | | | $n$ | ($x\pm s$) | $n$ | ($x\pm s$) | $n$ | ($x\pm s$) |
| 1 | Bulk | 50–5280 | 128 | 3.6±2.9 | 176 | 0.7±1.8 | 16 | 1.5±0.8 |
| | Shallow | 50–550 | 44 | 0.6±2.0 | 77 | −0.2±1.9 | 4 | 0.7±0.3 |
| | Intermediate | 550–1810 | 40 | 3.8±2.0 | 58 | 1.1±1.6 | 6 | 1.2±0.8 |
| | Deep | 1810–3890 | 29 | 6.3±1.0 | 35 | 1.8±1.2 | 5 | 2.2±0.1 |
| | Bottom | 3890–5280 | 15 | 6.3±1.2 | 6 | 1.6±1.1 | 1 | 2.9±0.0 |
| 2 | Bulk | 50–5280 | 128 | 0.5±1.7 | 176 | 0.4±1.7 | 16 | −0.1±0.6 |
| | Shallow | 50–550 | 44 | 0.3±1.9 | 77 | −0.2±1.9 | 4 | 0.1±0.0 |
| | Intermediate | 550–1810 | 40 | 0.9±1.7 | 58 | 0.8±1.5 | 6 | −0.2±0.5 |
| | Deep | 1810–3890 | 29 | 0.4±1.6 | 35 | 0.8±1.4 | 5 | −0.3±0.7 |
| | Bottom | 3890–5280 | 15 | −0.3±0.8 | 6 | 0.4±0.5 | 1 | 1.1±0.0 |

The data are grouped as follows: Pacific–East Indian (PEI), Atlantic–West Indian (AWI), and the Southern Ocean (SO).

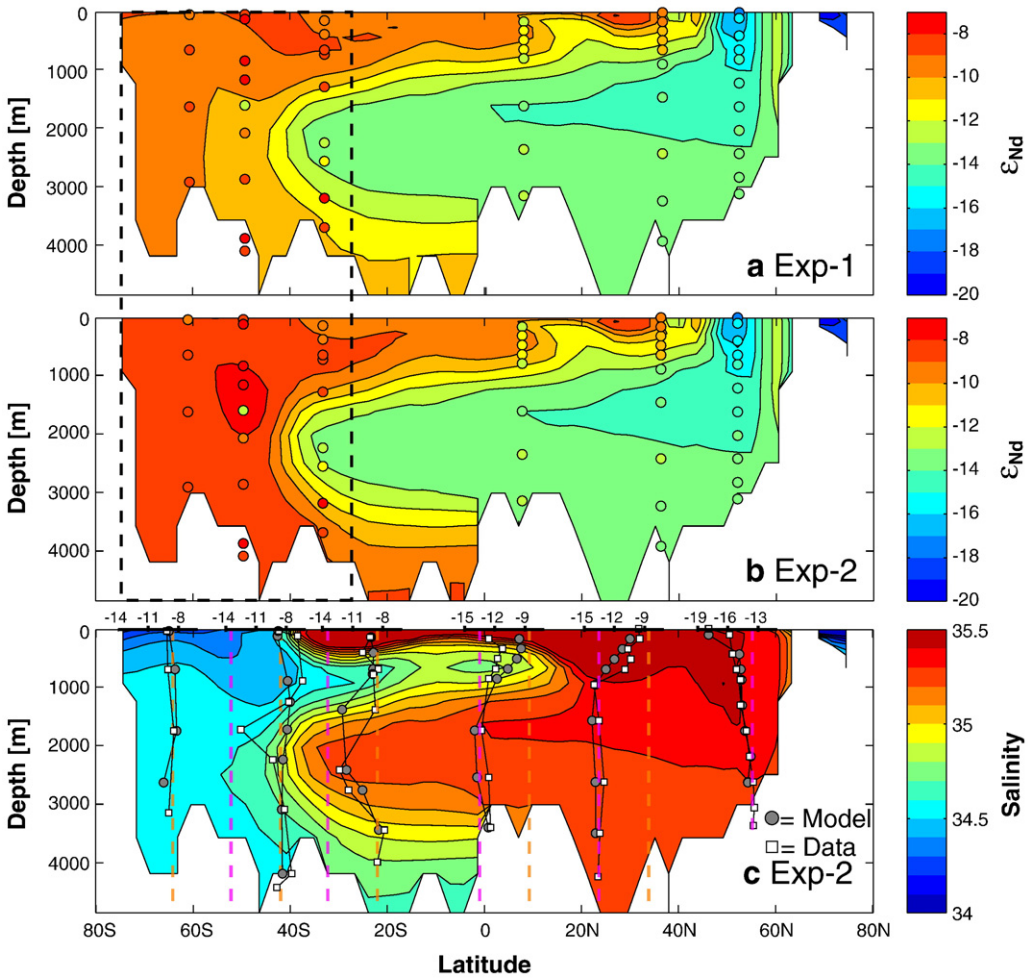


**Fig. 4.** $\varepsilon_{Nd}$ cross-sections of the Western Atlantic Basin for Exp-1 (panel a) and Exp-2 (panel b) with literature data superimposed as circles colored using the colorbar to the right of the plot. Panel c shows a model produced salinity cross-section for the Western Atlantic Basin with profiles of the modeled and measured data superimposed. The box encapsulating the southern portion of panels a and b highlights the offset between the model and data for Exp-1 and the elimination of this offset in Exp-2. The orange and purple dashed lines in panel c are represent typical deep water [$\varepsilon_{Nd}$] values for Southern and Northern source deep waters or −8.5 and −13.5, respectively.

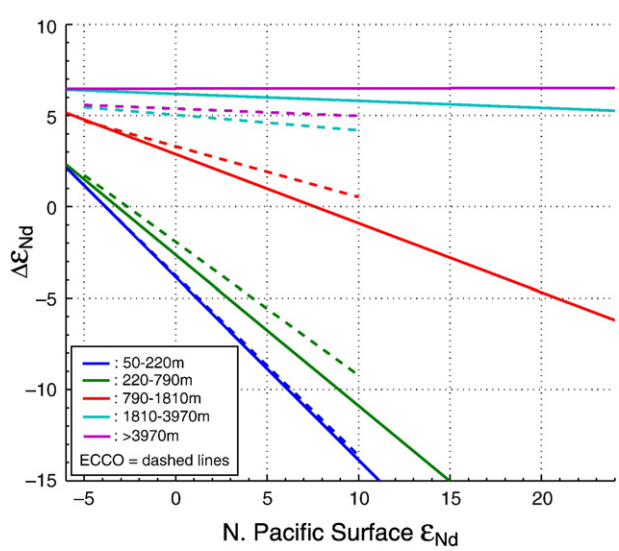


**Fig. 5.** Results for a sensitivity test showing $\Delta\varepsilon_{Nd}$ for various depth layers versus the $\varepsilon_{Nd}$ values defined for the surface North Pacific Ocean (North of 20'N). Both the 2.8° model (solid lines) and the 1° ECCO model (dashed lines) exhibit very similar sensitivities.

Pacific that is higher than what has been observed anywhere in the ocean to date ($\varepsilon_{Nd}$~+7.5) to eliminate the offset between the model simulations and data. However, a surface $\varepsilon_{Nd}$ value of +7.5 creates strongly negative $\Delta\varepsilon_{Nd}$ values for the surface ($\Delta\varepsilon_{Nd}$~−11) and NPIW ($\Delta\varepsilon_{Nd}$~−10) depth ranges. The deep waters of the OGCM (1810–3890 m) are minimally sensitive (slope~−0.04), and those for the bottom (>3890 m) are not at all sensitive (slope~0.00) to the interpolated $\varepsilon_{Nd}$ values of the surface North Pacific. To eliminate the offset between observed and simulated values in the deep Pacific Ocean (1810–3870 m) the surface Pacific would need to have an $\varepsilon_{Nd}$ value outside the range of what has been observed on Earth.

### 4.3. Sensitivity to model circulation

To evaluate the sensitivity of our results to the model circulation, we also carried out experiments using a TM derived from the ECCO-GODAE version of the MIT GCM. Specifically, the surface interpolation from Section 4.1 was interpolated onto the ECCO surface ocean layer and interior distributions were calculated. The ECCO-derived TM utilizing the interpolation from Section 4.1 was unable to exactly recreate the $\varepsilon_{Nd}$ value for NADW, but instead was ~2 $\varepsilon$-units too low. In order to recreate the observed values for NADW any attempt to create a "realistic" interpolation was abandoned and the surface North Atlantic Ocean was set to a value of −13.5 to ensure a reasonable value for NADW.

The ECCO model yields slightly lower deep and bottom water values for the entire ocean, but the difference is a nearly constant offset

of ~−0.85 $\varepsilon_{Nd}$ units (Fig. 5). We also mimicked the sensitivity test in Section 4.2 with the ECCO TM, but varied the surface Pacific (North of 20°N) between −5 and +10, in 5 $\varepsilon$-unit increments. The ECCO results exhibit very similar sensitivity to the coarser GCM. However, the depth ranges for NPIW (220–790 m) and intermediate waters (790–1810 m) in the ECCO model are slightly less sensitive to the interpolated North Pacific, while the deep and bottom depth ranges are somewhat more sensitive to the North Pacific surface ocean. In both models, the $\varepsilon_{Nd}$ value for the surface ocean would need to be ~+70, or greater to erase the offset between the data and model in the depth range of PDW.

### *4.4. Experiment 2: addition of a large reservoir of radiogenic Nd in the deep Pacific Ocean*

The results from our first experiment (Section 4.1) and initial sensitivity test (Section 4.2) suggest that an internal source of radiogenic Nd in the deep Pacific Ocean is required to balance the Nd isotope budget in the ocean. In a second set of experiments (Exp-2), we force the most of the non-surface Pacific Ocean to have $\varepsilon_{Nd}$ values consistent with the global high $\varepsilon_{Nd}$ end-member by imposing an additional boundary condition.

We constructed our reservoir of high $\varepsilon_{Nd}$ waters to correspond to a large volume of the Pacific Ocean where there exist significant positive $\Delta\varepsilon_{Nd}$ values in the first experiment. We defined the boundaries of deep waters of the Pacific using dissolved oxygen and silicate concentrations because they are good primary and secondary tracers of flow in this ocean basin at depth (Reid, 1997). These datasets were downloaded from the World Ocean Atlas and interpolated onto our model grid (Garcia et al., 2006b,a). All grid boxes with dissolved oxygen concentrations lower than 3.7 (mL/L) and with dissolved silicate concentrations higher than 80 (μmol/L) were set to an $\varepsilon_{Nd}$ value of −4.0. These dissolved oxygen and silicate concentrations were chosen because they resulted in the best agreement between the modeled and observed data. The sensitivity of the model results to the

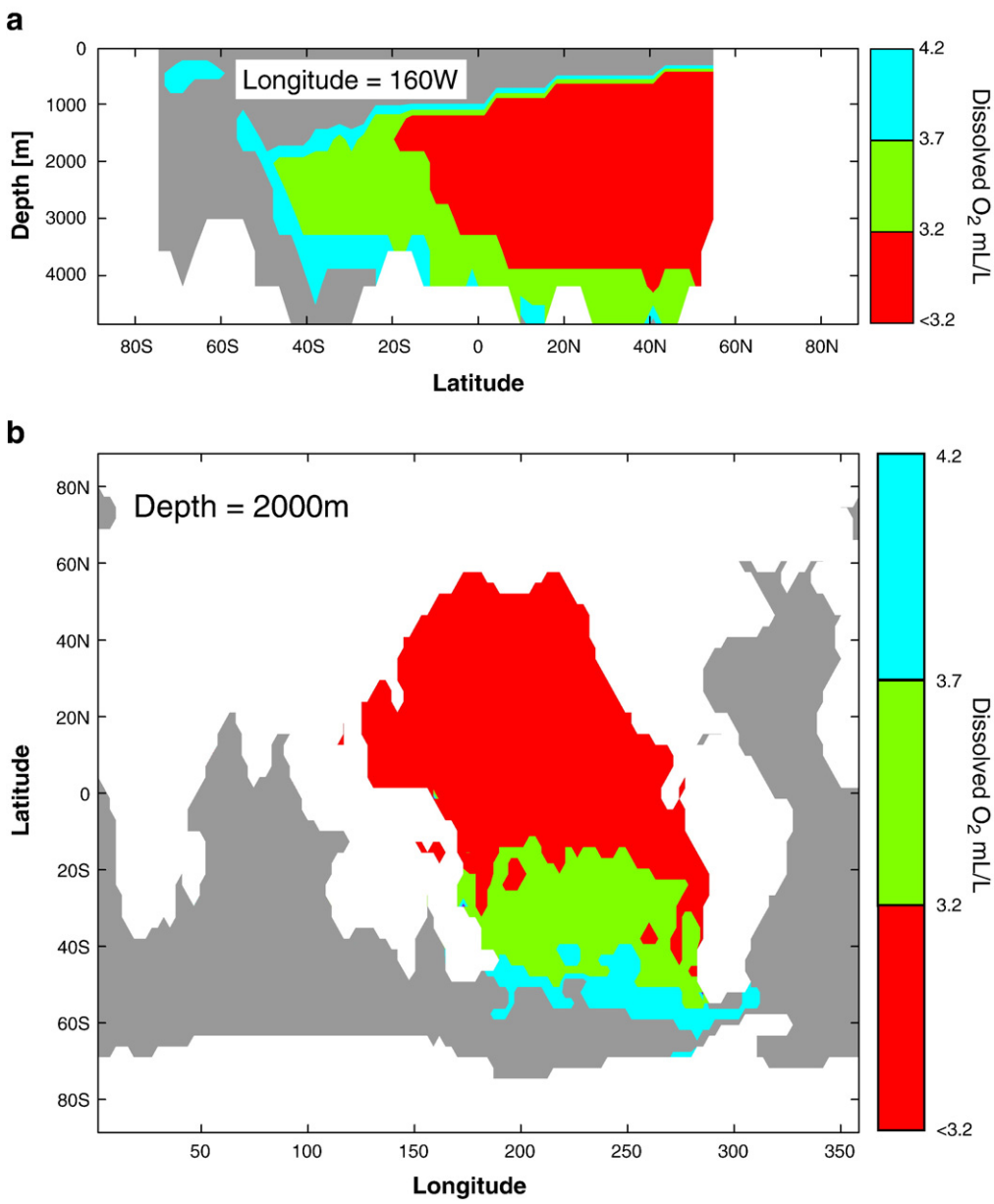


**Fig. 6.** a) The vertical extent of the deep Pacific source with cross-sections along longitude 160°W, for dissolved oxygen concentrations of 3.2, 3.7 and 4.2 mL/L where dissolved silicate concentrations greater than 80 μmols/L. b) The horizontal extents of the deep Pacific source at 2000 m depth for dissolved oxygen concentrations of 3.2, 3.7 and 4.2 mL/L where dissolved silicate concentrations greater than 80 μmols/L.

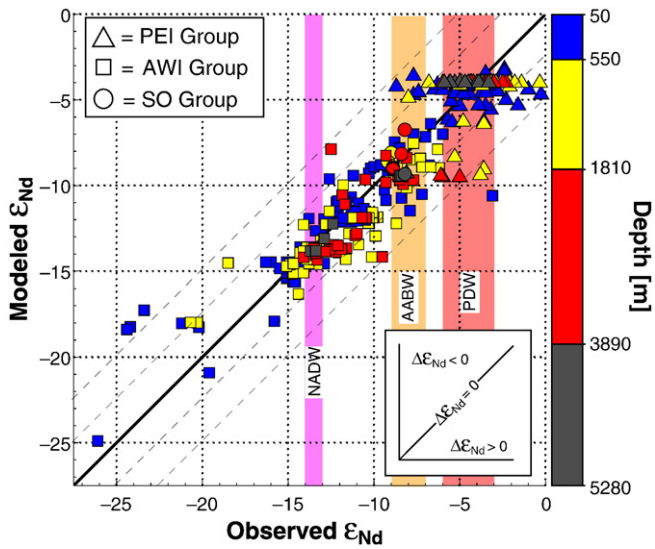


**Fig. 7.** Observed $\varepsilon_{Nd}$ versus modeled $\varepsilon_{Nd}$ of Exp-2 for model grid points from depths greater than 50 m for all datasets (PEI, AWI and SO) and color-coded according to depth. The addition of a high $\varepsilon_{Nd}$ source in the deep Pacific Ocean brings all $\Delta\varepsilon_{Nd}$ values for the deep and bottom PEI group to within 2.5 $\varepsilon$-units of the equiline. The $\Delta\varepsilon_{Nd}$ values for the deep and bottom SO group and AWI samples with measured $\varepsilon_{Nd}$ values similar to that exported from the Southern Ocean are also moved toward the equiline.

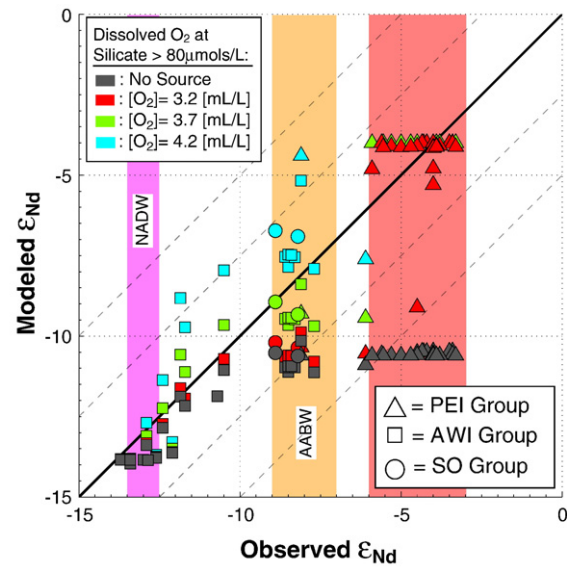


**Fig. 9.** Observed $\varepsilon_{Nd}$ versus modeled $\varepsilon_{Nd}$ with different dissolved $O_2$ concentration thresholds for model grid points with dissolved silicate concentrations greater than 80 μmol/L at depths greater than 2500 m.

concentrations of dissolved oxygen and silicate are shown later, in Section 4.4.

The dissolved oxygen and silicate thresholds (3.7 mL/L and 80 μmol/L, respectively) define an internal source region that has a depth ranging from ~200 m to the ocean bottom. Its depth range gradually thins out in the South Pacific Ocean (Fig. 6a). The maximum horizontal extent of the internal source occurs at a depth of approximately 2000 m, spans the entire width of the Pacific Ocean basin and extends from the northern edge of the basin to 45°S, near Australia and New Zealand, to 58°S near the tip of South America (Fig. 6b). The $\varepsilon_{Nd}$ value of −4.0 was chosen because it is representative of the deep and bottom depth ranges of the North Pacific.

With the addition of the radiogenic source of Nd in the deep Pacific Ocean, more than 91% of the global model results fall within 3.0 $\varepsilon$-units of the measured seawater data, and more than 50% are within 1.0 $\varepsilon$-unit (Fig. 7). The bulk mean of $\Delta\varepsilon_{Nd}$ values the PEI group is brought to within one standard deviation of zero (mean = 0.5 ± 1.7) and the $\Delta\varepsilon_{Nd}$ values conform to a normal distribution (Fig. 8b). Moreover, the mean $\Delta\varepsilon_{Nd}$ values of all individual depth ranges of the PEI data group are brought to within 1.0 $\varepsilon$-unit of zero (Table 1).

The addition of an internal radiogenic source to the Pacific end-member also brings the mean $\Delta\varepsilon_{Nd}$ values for the AWI and SO groups closer to zero. The $\Delta\varepsilon_{Nd}$ values calculated for the AWI remain normally distributed, and the means for the deep and bottom depth ranges are moved to within one $\varepsilon$-unit of zero ($mean_{deep}$ = 0.8 ± 1.4, $mean_{bottom}$ = 0.4 ± 0.5; Fig. 2c). In addition, the mean of $\Delta\varepsilon_{Nd}$ values from every depth level of the SO group are brought to closer zero (Table 1).

The results for Exp-2, which include a deep Pacific high $\varepsilon_{Nd}$ reservoir, are sensitive to the geographic extent of that reservoir and subtle changes to the dissolved oxygen concentration threshold used to define this reservoir led to differences in the model results (Figs. 6a, b and 9). Basing the high $\varepsilon_{Nd}$ reservoir on a low dissolved oxygen threshold of 3.2 mL/L decreases its geographic extent, and results in positive $\Delta\varepsilon_{Nd}$ values for the Southern Ocean and for the

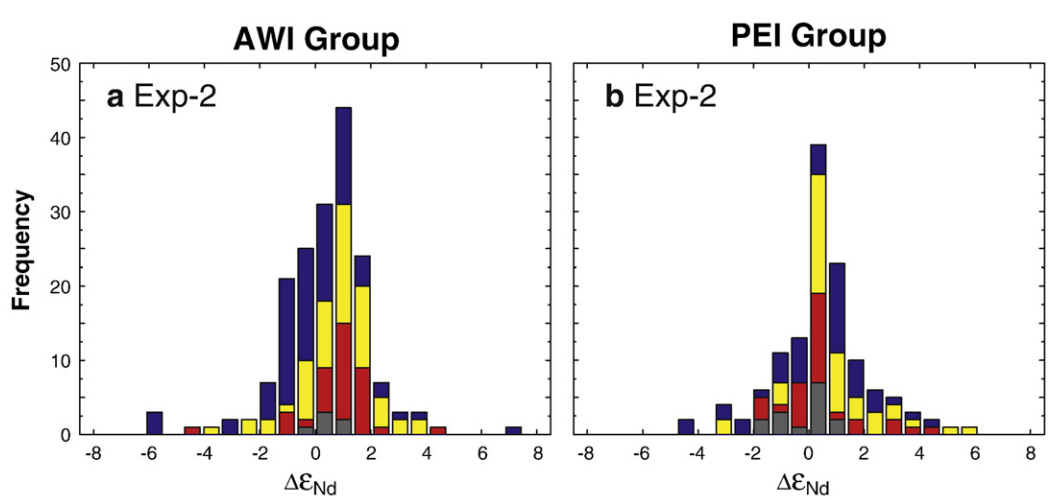


**Fig. 8.** Grouped histograms of model results showing the distributions of $\Delta\varepsilon_{Nd}$ values [$\Delta\varepsilon_{Nd} = \varepsilon_{Nd}$(observed) − $\varepsilon_{Nd}$(modeled)] for AWI (panel a) and PEI datasets (panel b) for Exp-2. The histograms are colored according to the depths listed in the text and shown in the color bar in Fig. 2 (shallow = blue; intermediate = yellow; deep = red; bottom = gray). Exp-2 involves the addition of a deep Pacific reservoir of radiogenic Nd.

waters exported from it, to values that are close to those obtained when the pacific source is excluded (Fig. 9). Conversely, increasing the dissolved oxygen concentration threshold to 4.2 mL/L increases its geographic extent leads to negative $\Delta\varepsilon_{Nd}$ values in the Southern Ocean (Fig. 9).

## 5. Discussion

In Exp-1 we made the simple assumption that inputs of Nd occur solely to the surface ocean and that the $\varepsilon_{Nd}$ values of seawater mix conservatively thereafter. We interpolate the entire surface ocean and treat this as a fixed boundary condition and calculated the resulting interior distribution. Our interpolation of $\varepsilon_{Nd}$ values for the surface ocean does not account for sources and sinks, but instead should be thought of as our best estimate of what a steady-state mixture of all surface sources of Nd would look like, if such a thing exists. Since we did not attempt to model all the sources and sinks of Nd in the surface ocean we cannot rule out that one or many processes, some of which may fall under the label of "boundary exchange" (Lacan and Jeandel, 2005a,b), play(s) a role in the creation of this pattern.

The results for Exp-1 (Section 4.1) suggest that there must be an internal source of Nd in the Pacific Ocean, or that the model circulation and/or surface interpolation are deficient. Subsequent sensitivity tests (Sections 4.2 and 4.3), in which the surface North Pacific Ocean is set with $\varepsilon_{Nd}$ values that include the highest observed on Earth, show that given the circulation constraints of the 2.8° TM, it is not possible to recreate the observed values by the conservative mixing of North Pacific surface waters. Very similar results were obtained with the 1° resolution, data-assimilated ECCO TM.

The specifics of the process adding radiogenic Nd to the deep Pacific Ocean is not currently known, but its source likely derives from Circum-Pacific volcanism. We note that the discrepancy seen in the Pacific Ocean extends to the eastern Indian Ocean. Meanwhile, the western Indian Ocean results do not show this discrepancy. The mismatch of model simulations and data in the eastern Indian Ocean indicates that either the Pacific discrepancy propagates into the eastern Indian Ocean, or that deep Indian Ocean water is tagged with an additional source of radiogenic Nd such as from Indonesian arcs (e.g. Jeandel et al., 1998). In the latter case, this may mean that proximity to volcanic arcs limits the quasi-conservative behavior of Nd isotopes in seawater.

In our model runs it was possible to recreate the $\varepsilon_{Nd}$ value for NADW, but this was sensitive to the interpolation scheme used to create the surface map of Nd isotopes in the North Atlantic Ocean, where the waters that form NADW derive. This is true in spite of relatively good data coverage in this region. The sensitivity of the modeled value of NADW most likely reflects the fact that there is a wide range of $\varepsilon_{Nd}$ values observed in the North Atlantic, as low as −26 in Baffin Bay and as high as −4 near Iceland. As a result, different interpolation schemes produce subtle differences in the geographic extents of high or low $\varepsilon_{Nd}$ values in the surface ocean that lead to differences in the modeled value of NADW. We draw no conclusions from the fact that we were able to reproduce Nd isotope ratios for NADW that are consistent with the observed values for this water mass. Instead, we want to focus on the fact that reproducing NADW $\varepsilon_{Nd}$ values is a necessary requirement in testing for internal sources in all other ocean basins, because NADW is an important constituent of global deep waters and represents an end-member Nd isotope composition of deep waters.

In our second experiment (Exp-2 Section 4.4), we added a reservoir of radiogenic Nd to the deep Pacific Ocean to satisfy the need for such a reservoir demonstrated in our first experiment (Exp-1 Section 4.1) and subsequent sensitivity tests (Section 4.2 and 4.3). Once this reservoir was added our simulated results were able to reproduce a majority of the variations in $\varepsilon_{Nd}$ values observed in the modern ocean. This result indicates that deep waters of areas intermediate to the NADW and PDW source regions are consistent with quasi-conservative mixing of these two end-members and that boundary exchange need not occur everywhere. Indeed, the results of this modeling study suggest that boundary exchange may be limited, with a few exceptions, to the Pacific. Areas of high turbidity and the submarine fans of large rivers in the Atlantic and Indian basins may be exceptions.

There are a number of possible processes by which radiogenic Nd may be delivered to the deep ocean, including reversible scavenging by particles sinking through the ocean, or a distributed source associated with the dissolution of volcanic ash and glass (e.g. Albarède and Goldstein, 1992). An effect of particle scavenging would be to smear the high Nd isotope values observed in the surface layer of the Pacific Ocean downward to the interior ocean. So, reversible scavenging is a process that can input Nd to the interior ocean through a process independent of conservative ocean circulation.

A possible issue with invoking reversible scavenging as the mechanism for an internal source in the Pacific Ocean is that this process would also occur in the Atlantic and in other ocean basins. However, the Atlantic and Pacific both show some unique characteristics that may be key to the apparent differential behavior of Nd in each ocean basin. The flushing time of the Western Atlantic is on the order of decades to centuries (Broecker et al., 1991; Smethie et al., 2000), while in the Pacific the residence time of deep waters is on order of several centuries (Matsumoto, 2007) and the relative stagnancy is compounded by the large amount of labile volcanic material delivered there. More modeling is needed, and an objective for future studies would be to accurately recreate the spatial variations in Nd isotopes and concentrations for the Pacific basin, identifying possible input mechanisms and ruling out others. Such work should go a long way toward increasing our understanding of sources of Nd in the oceans' interior.

## 6. Conclusions

This paper presents results for modeling the distribution of Nd isotopes in the oceans using an OGCM. Initial runs were performed using interpolated surface Nd isotopic compositions as fixed boundary condition, upon which transport and mixing according to the flow characteristics of the OGCM acted until the interior ocean reached steady state. This approach was taken because it mimics the behavior of the well-understood conservative tracers, potential temperature and salinity, which should maximize the interpretability of our results. The results show that the first order assumption of quasi-conservative behavior of Nd isotopes as a tracer can reproduce much of the Nd isotope variation in the modern oceans, as long as an internal source of radiogenic Nd in the Pacific is imposed. The weak sensitivity of the simulated Nd isotope ratios in the deep Pacific Ocean to the surface values in the North Pacific, in both the 2.8° and 1° models, suggests that this is a robust result.

We did not model the process adding radiogenic Nd to the deep Pacific Ocean. However, exchange between seawater and sediments at depth, or exchange at the surface and subsequent downward mixing by reversible scavenging on particles in the open ocean or at the boundaries likely plays some role. If particle scavenging is the primary process delivering the high $\varepsilon_{Nd}$ signal to the deep Pacific from the surface, then our result of apparent conservative behavior of Nd isotopes in the Atlantic might be reconciled with the lack of conservative behavior in the Pacific by recognizing the difference in flushing times for each ocean basin (short in the Atlantic and longer in the Pacific) and the prevalence of volcanic terrains around the Pacific Ocean basin.

Our results strongly suggest that radiogenic Nd is added to the deep Pacific Ocean through a process other than simple ocean circulation (advection and diffusion) of surface inputs. An influx of data from the entire Pacific Ocean basin along with additional modeling studies focusing on processes that can replicate the observed distribution of $\varepsilon_{Nd}$ and rare earth element concentrations in the Pacific Ocean will go a long way toward increasing our understanding of the

marine Nd cycle in both the modern and ancient oceans, and will aid in the interpretation of Nd isotope records in marine archives.

## Acknowledgements

This project was started as a result of the Nd modeling seminar at LDEO. We would also like to acknowledge Mark Siddall for valuable discussions and Mohi Kumar for help in the editing of this manuscript. This work is partially funded by NSF grant OCE 05-26884 to SLG and SRH. SK's contribution was funded by NSF grant OCE-0623366. This is LDEO contribution #7168.

## References

Albarède, F., Goldstein, S.L., 1992. World map of nd isotopes in sea-floor ferromanganese deposits. Geology 20, 761–763.
Amakawa, H., Nozaki, Y., Alibo, D.S., Zhang, J., Fukugawa, K., Nagai, H., 2004. Neodymium isotopic variations in northwest pacific waters. Geochim. Cosmochim. Acta 68, 715–727.
Arsouze, T., Dutay, J.C., Lacan, F., Jeandel, C., 2007. Modeling the neodymium isotopic composition with a global ocean circulation model. Chem. Geol. 239, 165–177.
Bearman, G. (Ed.), 2002. Ocean circulation. Butterworth-Heinemann, Boston. 286 pp.
Bertram, C.J., Elderfield, H., 1993. The geochemical balance of the rare-earth elements and neodymium isotopes in the oceans. Geochim. Cosmochim. Acta 57, 1957–1986.
Broecker, W.S., Peng, T.-H., 1982. Tracers in the sea. Eldigio Press, Palisades, NY.
Broecker, W.S., Blanton, S., Smethie, W., Ostlund, G., 1991. Radiocarbon decay and oxygen utilization in the deep Atlantic ocean. Glob. Biogeochem. Cycles 5, 87–117.
Conkright, M., Levitus, S., O'Brien, T., Boyer, T., Anotonov, J., Stephens, C., 1998a. World ocean atlas 1998 cd-rom data set documentation. Tech. Rep. 15, nodc internal report. National Oceanographic Data Center, Silver spring, MD. 16pp.
Conkright, M.E., O'Brien, T.D., Levitus, S., Boyer, T.P., Stephens, C., 1998b. World ocean atlas 1998 vol. 10: Nutrient and chlorophyll of the Atlantic ocean. Noaa atlas nesdis 36. U.S. Government printing office, Washington, D.C.
Dutay, J.C., Bullister, J.L., Doney, S.C., Orr, J.C., Najjar, R., Caldeira, K., Campin, J.M., Drange, H., Follows, M., Gao, Y., Gruber, N., Hecht, M.W., Ishida, A., Joos, F., Lindsay, K., Madec, G., Maier-Reimer, E., Marshall, J.C., Matear, R.J., Monfray, P., Mouchet, A., Plattner, G.K., Sarmiento, J., Schlitzer, R., Slater, R., Totterdell, I.J., Weirig, M.F., Yamanaka, Y., Yool, A., 2002. Evaluation of ocean model ventilation with cfc-11: Comparison of 13 global ocean models. Ocean Model. 4, 89–120.
Frank, M., 2002. Radiogenic isotopes: tracers of past ocean circulation and erosional input. Rev. Geophys. 40, 38.
Garcia, H.E., Locarnini, R.A., Boyer, T.P., Antonov, J.I., 2006a. Volume 4: nutrients (phosphate, nitrate, silicate). In: Levitus, S. (Ed.), World Ocean Atlas 2005, NOAA Atlas NESDIS 63, U.S. Government Printing Office, Washington D.C., p. 396.
Garcia, H.E., Locarnini, R.A., Boyer, T.P., Antonov, J.I., 2006b. Volume 3: dissolved oxygen, apparent oxygen utilization, and oxygen saturation. In: Levitus, S. (Ed.), World Ocean Atlas 2005, NOAA Atlas NESDIS 63. U.S. Government Printing Office, Washington D.C., p. 342.
Gent, P.R., McWilliams, J.C., 1990. Isopycnal mixing in ocean circulation models. J. Phys. Oceanogr. 20, 150–155.
Goldstein, S.L., Hemming, S.R., 2003. Long-lived isotopic tracers in oceanography, paleoceanography and ice sheet dynamics. Elsevier, Oxford.
Goldstein, S.L., O'Nions, R.K., 1981. Nd and Sr isotopic relationships in pelagic clays and ferromanganese deposits. Nature 292, 324–327.
Jacobsen, S.B., Wasserburg, G.J., 1980. Sm-nd isotopic evolution of chondrites. Earth Planet. Sci. Lett. 50, 139–155.
Jeandel, C., 1993. Concentration and isotopic composition of Nd in the South-Atlantic ocean. Earth Planet. Sci. Lett. 117, 581–591.
Jeandel, C., Thouron, D., Fieux, M., 1998. Concentrations and isotopic compositions of neodymium in the eastern indian ocean and indonesian straits. Geochim. Cosmochim. Acta 62, 2597–2607.
Jiang, S., Stone, P.H., Malanotte-Rizzoli, P., 1999. An assessment of the geophysical fluid dynamics laboratory ocean model with coarse resolution: annual-mean climatology. J. Geophys. Res.-Oceans 104, 25623–25645.
Johannesson, K.H., Burdige, D.J., 2007. Balancing the global oceanic neodymium budget: evaluating the role of groundwater. Earth Planet. Sci. Lett. 253, 129–142.
Jones, C.E., Halliday, A.N., Rea, D.K., Owen, R.M., 1994. Neodymium isotopic variations in north pacific modern silicate sediment and the insignificance of detrital ree contributions to seawater. Earth Planet. Sci. Lett. 127, 55–66.
Khatiwala, S., 2007. A computational framework for simulation of biogeochemical tracers in the ocean. Glob. Biogeochem. Cycles 21, 14.
Khatiwala, S., Visbeck, M., Cane, M.A., 2005. Accelerated simulation of passive tracers in ocean circulation models. Ocean Model. 9, 51–69.
Lacan, F., Jeandel, C., 2005a. Neodymium isotopes as a new tool for quantifying exchange fluxes at the continent-ocean interface. Earth Planet. Sci. Lett. 232, 245–257.
Lacan, F., Jeandel, C., 2005b. Acquisition of the neodymium isotopic composition of the north Atlantic deep water. Geochem. Geophys. Geosyst. 6, 20.
Marshall, J., Adcroft, A., Hill, C., Perelman, L., Heisey, C., 1997. A finite-volume, incompressible navier stokes model for studies of the ocean on parallel computers. J. Geophys. Res.-Oceans 102, 5753–5766.
Martin, E.E., Scher, H.D., 2004. Preservation of seawater Sr and Nd isotopes in fossil fish teeth: bad news and good news. Earth Planet. Sci. Lett. 220, 25–39.
Matsumoto, K., 2007. Radiocarbon-based circulation age of the world oceans. J. Geophys. Res.-Oceans 112.
Matsumoto, K., Sarmiento, J.L., Key, R.M., Aumont, O., Bullister, J.L., Caldeira, K., Campin, J.M., Doney, S.C., Drange, H., Dutay, J.C., Follows, M., Gao, Y., Gnanadesikan, A., Gruber, N., Ishida, A., Joos, F., Lindsay, K., Maier-Reimer, E., Marshall, J.C., Matear, R.J., Monfray, P., Mouchet, A., Najjar, R., Plattner, G.K., Schlitzer, R., Slater, R., Swathi, P.S., Totterdell, I.J., Weirig, M.F., Yamanaka, Y., Yool, A., Orr, J.C., 2004. Evaluation of ocean carbon cycle models with data-based metrics. Geophys. Res. Lett. 31.
Nakai, S., Halliday, A.N., Rea, D.K., 1993. Provenance of dust in the Pacific-ocean. Earth Planet. Sci. Lett. 119, 143–157.
Piepgras, D.J., Jacobsen, S.B., 1988. The isotopic composition of neodymium in the North Pacific. Geochim. Cosmochim. Acta 52, 1373–1381.
Piepgras, D.J., Wasserburg, G.J., 1980. Neodymium isotopic variations in seawater. Earth Planet. Sci. Lett. 50, 128–138.
Piepgras, D.J., Wasserburg, G.J., 1982. Isotopic composition of neodymium in waters from the drake passage. Science 217, 207–214.
Piepgras, D.J., Wasserburg, G.J., 1983. Influence of the mediterranean outflow on the isotopic composition of neodymium in waters of the North-Atlantic. J. Geophys. Res.-Oceans Atmos. 88, 5997–6006.
Piepgras, D.J., Wasserburg, G.J., 1987. Rare-earth element transport in the western North-Atlantic inferred from Nd isotopic observations. Geochim. Cosmochim. Acta 51, 1257–1271.
Piepgras, D.J., Wasserburg, G.J., Dasch, E.J., 1979. Isotopic composition of Nd in different ocean masses. Earth Planet. Sci. Lett. 45, 223–236.
Piotrowski, A.M., Goldstein, S.L., Hemming, S.R., Fairbanks, R.G., 2004. Intensification and variability of ocean thermohaline circulation through the last deglaciation. Earth Planet. Sci. Lett. 225, 205–220.
Piotrowski, A.M., Goldstein, S.L., Hemming, S.R., Fairbanks, R.G., 2005. Temporal relationships of carbon cycling and ocean circulation at glacial boundaries. Science 307, 1933–1938.
Reid, J.L., 1997. On the total geostrophic circulation of the pacific ocean: flow patterns, tracers, and transports. Progr. Oceanogr. 39, 263–352.
Rutberg, R.L., Hemming, S.R., Goldstein, S.L., 2000. Reduced North Atlantic deep water flux to the glacial southern ocean inferred from neodymium isotope ratios. Nature 405, 935–938.
Sandwell, D.T., 1987. Biharmonic spline interpolation of geos-3 and seasat altimeter data. Geophys. Res. Lett. 14, 139–142.
Schlosser, P., Bullister, J.L., Fine, R., Jenkim, W.J., Key, R., Lupton, J., Roether, W., Smethie, W.M.J., 2001. In: Siedler, G., Church, J., Gould, J. (Eds.), Ocean circulation and climate: Observing and modelling the global ocean. Academic Press, pp. 431–452.
Shimizu, H., Tachikawa, K., Masuda, A., Nozaki, Y., 1994. Cerium and neodymium isotope ratios and ree patterns in seawater from the North Pacific-Ocean. Geochim. Cosmochim. Acta 58, 323–333.
Smethie, W.M., Fine, R.A., Putzka, A., Jones, E.P., 2000. Tracing the flow of north Atlantic deep water using chlorofluorocarbons. J. Geophys. Res.-Oceans 105, 14297–14323.
Tachikawa, K., Jeandel, C., Roy-Barman, M., 1999. A new approach to the Nd residence time in the ocean: the role of atmospheric inputs. Earth Planet. Sci. Lett. 170, 433–446.
Tachikawa, K., Athias, V., Jeandel, C., 2003. Neodymium budget in the modern ocean and paleo-oceanographic implications. J. Geophys. Res.-Oceans 108, 13.
Tazoe, H., Obata, H., Gamo, T., 2006. Vertical profiles of cerium and neodymium compositions and rees pattern in the ross sea. Goldschmidt Geochemistry Conference.
Trenberth, K., J., O., W., L., 1989. A global wind stress climatology based on ECMWF analyses. Tech rep. Ncar/tn-338+str. National Center for Atmospheric Research.
Vance, D., Scrivner, A.E., Beney, P., Staubwasser, M., Henderson, G.M., Slowey, N.C., 2004. The use of foraminifera as a record of the past neodymium isotope composition of seawater. Paleoceanography 19, 17.
van de Flierdt, T., Frank, M., Lee, D.C., Halliday, A.N., Reynolds, B.C., Hein, J.R., 2004. New constraints on the sources and behavior of neodymium and hafnium in seawater from Pacific Ocean ferromanganese crusts. Geochim. Cosmochim. Acta 68, 3827–3843.
van de Flierdt, T., Robinson, L.F., Adkins, J.F., Hemming, S.R., Goldstein, S.L., 2006. Temporal stability of the neodymium isotope signature of the holocene to glacial North Atlantic. Paleoceanography 21, 6.
Wunsch, C., Heimbach, P., 2007. Practical global oceanic state estimation. Phys. D-Nonlinear Phenom. 230, 197–208.